Insight Into the Stability and Electronic and Optical Properties of N-Heterocyclic Carbene Analogues of Halogen/Phosphine-Protected Au-13 Superatomic Clusters

Jianyu Wei, Samia Kahlal, Jean-François Halet, Jean-Yves Saillard, Alvaro Munoz-Castro

Insight into the Stability, Electronic and Optical Properties of N-Heterocyclic Carbene Analogues of Halogen/Phosphine Protected Au_{13} *Superatomic* Clusters

Jianyu Wei,[a] *Samia Kahlal,*[a] *Jean-François Halet,* [b]* *Jean-Yves Saillard*[a]* *and Alvaro Muñoz-Castro*[c]*

[a] Univ Rennes, CNRS, Institut des Sciences Chimiques de Rennes (ISCR) – UMR 6226, F-35000 Rennes, France

[b] CNRS–Saint-Gobain–NIMS, IRL 3629, Laboratory for Innovative Key Materials and Structures (LINK), National Institute for Materials Science (NIMS), Tsukuba, 305-0044, Japan

[c] Grupo de Química Inorgánica y Materiales Moleculares, Facultad de Ingenieria, Universidad Autonoma de Chile, El Llano Subercaseaux 2801, Santiago, Chile

Abstract

Atomically-precise gold nanoclusters (AuNCs) belong to a relevant area offering useful templates with tunable properties towards functional nanostructures. In this work, we explored the feasible incorporation of N-heterocyclic carbenes (NHCs), as part of the protecting-ligand shell in AuNCs. Our results based on the substitution of phosphine ligands in experimentally characterized AuNCs by NHCs in various 8-electron *superatoms* Au_{13} and M_4Au_9 (M = Cu, Ag) indicate similar electronic structure and stability, but somewhat different optical properties. These findings support the feasible obtention of novel targets for explorative synthetic efforts featuring NHC-ligands on medium-sized species based on the recurrent Au_{13} icosahedral core. The hypothetical species appear to be interesting templates for building blocks in nanostructured materials with tuned properties, which encourage experimental exploration of ligand-versatility in homo and heterometallic *superatomic* clusters.

*****Dedicated to our colleague and friend Professor Didier Astruc on the occasion of his 75th birthday.

Emails:

Jean-Francois.Halet@univ-rennes1.fr

saillard@univ-rennes1.fr

alvaro.munoz@uautonoma.cl

1. Introduction

Atomically precise gold nanoclusters (AuNCs) have been the subject of intense research over the past decade[1–6] owing to their potential use in emerging technological applications.[7–15] Their unique molecule-like and size-dependent properties, as well as their rich structural diversity,[1,16–23] provide the opportunity to design new species, opening new opportunities for tailorable applications.[8,24,33–37,25–32] The AuNC structures are generally composed of a central metallic core, protected (passivated) by various ligands.[29,38–41] The Au_{13}-centered icosahedron is one of the most recurrent core motifs. It was first characterized in $[Au_{13}(PPhMe_2)_{10}Cl_2]^{3+}$ by Mingos and coworkers,[42] and later in the extensive research on $[Au_{25}(SR)_{18}]^-$ species.[37,43–46]

The central metallic core exhibits particular electronic and structural features accounting for the stability of the overall cluster,[47–52] with a specific number of bonding cluster electrons (*ce*), *i.e.*, electrons provided by the 6s(Au) orbitals. For example, the Au_{13}^{5+} core of $[Au_{13}(PPhMe_2)_{10}Cl_2]^{3+}$ is an 8-*ce* species with a $1S^2\ 1P^6$ electronic structure according to the *superatom* model.[29,53,54] The highest occupied and lowest unoccupied molecular orbitals (HOMO and LUMO) correspond to the $1P^6$ and $1D^0$ shells, respectively.[29,53,54] Furthermore, different synthetic strategies allow further exploration of the versatility of the cluster stability and properties by varying the number and nature of its attached ligands. For example, the classical $[Au_{13}(dppe)_5Cl_2]^{3+}$ (dppe = 1,2-bis(diphenylphosphino)ethane) possesses enhanced optical, luminescent, and singlet-oxygen sensitization capabilities, as reported by Konishi and Li.[55,56] Whereas this cluster is decorated with two Cl atoms, the number of chlorides can be increased to three or four.[56] In addition, the $Au_{13}Cl_4$ species has been shown to have related $Au_{13}Br_4$ and $Au_{13}I_4$ counterparts.[57]

Moreover, the recent incorporation of N-heterocyclic carbenes (NHC) as neutral ligands of gold AuNCs,[58] as reported for the related $[Au_{13}(NHC)_9Cl_3]^{2+}$ cluster by Crudden and coworkers,[59] and which displays a high emission quantum yield, allows further development of more versatile ligands owing to the central role of NHC ligands in organometallic chemistry.[60–66] Hence, their evaluation and comparison to phosphines may encourage further ligand engineering efforts and synthetic exploration of such species,[67,68,77–80,69–76] offering the opportunity of tuning nanocluster properties.

We have recently shown from density functional theory (DFT) calculations that NHCs are at least as efficient as phosphines for stabilizing AuNCs of small size and that they should exhibit somewhat related optical properties.[81] In this work, we extend our investigations to the

substitution of phosphine ligands by NHCs in a wide series of experimentally characterized halogen/phosphine-protected *8-ce superatomic* Au_{13} and M_nAu_{13-n} clusters (M = Cu, Ag, Pd). This work mainly focuses on the substitution-induced change of the stability, electronic structure, and optical (including emissive) properties. Meanwhile, the influence of changing of the type and number of halogen ligands is also investigated for both the phosphine- and NHC-protected analogues. The considered halogen/phosphine-protected Au_{13} series are composed of the experimentally characterized compounds as follows, $[Au_{13}(PPhMe_2)_{10}Cl_2]^{3+}$ (**$Au_{13}Cl_2$-P'**),[42] $[Au_{13}(dppe)_5Cl_2]^{3+}$ (**$Au_{13}Cl_2$-P'e**),[56] $[Au_{13}(PMePh_2)_9Cl_3]^{2+}$ (**$Au_{13}Cl_3$-P'**),[57] $[Au_{13}(PMePh_2)_8Cl_4]^{+}$ (**$Au_{13}Cl_4$-P'**),[82] $[Au_{13}(dppp)_4Cl_4]^{+}$ (**$Au_{13}Cl_4$-P'p**),[83,84] $[Cu_4Au_9(PMePh_2)_8Cl_4]^{+}$ (**$Cu_4Au_9Cl_4$-P'**),[82] $[Ag_4Au_9(PMePh_2)_8Cl_4]^{+}$ (**$Ag_4Au_9Cl_4$-P'**),[82] $[PdAu_{12}(dppe)(PPh_3)_6Cl_4]$ (**$PdAu_{12}Cl_4$-P'/P'e**),[44] $[Au_{13}(PMePh_2)_8Br_4]^{+}$ (**$Au_{13}Br_4$-P'**),[57] and $[Au_{13}(PMePh_2)_8I_4]^{+}$ (**$Au_{13}I_4$-P'**) (dppp = 1,3-bis(diphenylphosphino)propane).[57] To better understand the role of the halogen ligands, the homoleptic non-halogenated $[Au_{13}(dppm)_6]^{5+}$ (**Au_{13}-P'm**) (dppm = 1,1-bis(diphenylphosphino)methane)[85,86] clusters was also included for comparison. All the investigated compounds are *8-ce superatoms*. Some of them contain di-phosphines (**P'm, P'e, P'p**), whereas others have simple phosphines (**P'**). Nevertheless, the X-ray and optical data are available for most of them. The hypothetical NHC homologues were designed by replacing the mono-phosphines by the mono-carbene N,N-diisopropylimidazolidene ligands (denoted as **NHC'** in the following), taken from the literature.[58,87] The dppm, dppe, and dppp ligands were substituted by NHC counterparts, namely 1,3-bis(N-isopropylimidazolidenyl)methane (**di-NHC'm**), 1,3-bis(N-isopropylimidazolidenyl)ethane (**di-NHC'e**) and 1,3-bis(N-isopropylimidazolidenyl)propane (**di-NHC'p**), respectively (see Scheme 1). These carbenes are representative of standard NHCs and exhibit realistic steric volumes. Thus, the computed hypothetical NHC clusters are $[Au_{13}(di\text{-}NHC'm)_6]^{5+}$ (**Au_{13}-C'm**), $[Au_{13}(NHC')_{10}Cl_2]^{3+}$ (**$Au_{13}Cl_2$-C'**), $[Au_{13}(di\text{-}NHC'e)_5Cl_2]^{3+}$ (**$Au_{13}Cl_2$-C'e**), $[Au_{13}(NHC')_9Cl_3]^{2+}$ (**$Au_{13}Cl_3$-C'**), $[Au_{13}(NHC')_8Cl_4]^{+}$ (**$Au_{13}Cl_4$-C'**), $[Au_{13}(di\text{-}NHC'p)_4Cl_4]^{+}$ (**$Au_{13}Cl_4$-C'p**), $[Cu_4Au_9(NHC')_8Cl_4]^{+}$ (**$Cu_4Au_9Cl_4$-C'**), $[Ag_4Au_9(NHC')_8Cl_4]^{+}$ (**$Ag_4Au_9Cl_4$-C'**), $[PdAu_{12}(di\text{-}NHC'e)(NHC')_6Cl_4]$ (**$PdAu_{12}Cl_4$-C'/C'e**), $[Au_{13}(NHC')_8Br_4]^{+}$ (**$Au_{13}Br_4$-C'**) and $[Au_{13}(NHC')_8I_4]^{+}$ (**$Au_{13}I_4$-C'**). See Table S1 (Supplementary Materials) for the full formula list of the investigated compounds and their corresponding abbreviations.

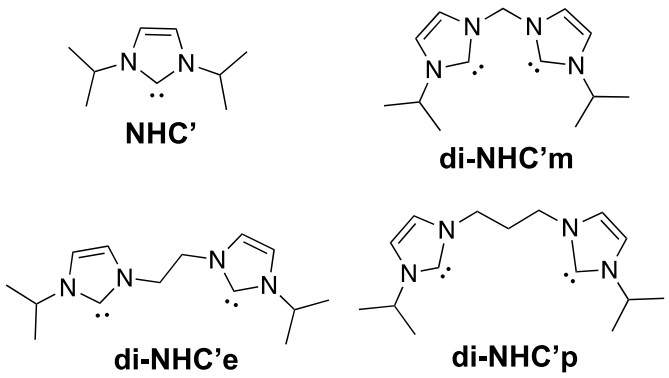

Scheme 1. The NHC ligands considered in this paper.

2. Computational Details

Geometry optimizations were performed at the DFT level using the Gaussian 16 package.[88] The Becke-Perdew exchange-correlation functional (BP86),[89,90] together with the Def2-SVP basis set,[91] which includes effective core potentials accounting for scalar relativistic effects, were used. Grimme's D3 empirical corrections[92] were included in order to take into account dispersion effects. All the optimized singlet ground states structures were confirmed as genuine minima on their potential energy surface by vibrational frequency calculations. The natural atomic orbital (NAO) populations and Wiberg bond indices (WBIs) were calculated using the NBO 6.0 program,[93] with the help of Amsterdam Density Functional code (ADF2017).[94,95] UV-vis optical transitions were computed using the time-dependent DFT (TD-DFT) method, at the B3LYP[96]/Def2-SVP level, which provided a good quantitative agreement with the experimental spectra, the deviations between the computed transitions and their corresponding experimental values being always less than 80 nm. The UV-vis spectra were simulated from the computed TD-DFT transition energies and their oscillator strengths by using the SWizard program,[97] with each transition being associated with a Gaussian function of half-height width equal to 2000 cm^{-1}. All the computed UV-vis transition wavelengths reported below correspond to individual computed transitions. To calculate the fluorescence emission wavelengths, the geometry of the excited singlet states were optimized by TD-DFT at the PBE0[98]/Def2-SVP level with the Gaussian16 program. To calculate the phosphorescence emission wavelengths, the triplet state geometries were firstly optimized by DFT calculations at the BP86/Def2-SVP level, and their energies, as well as those of their corresponding singlets, were recalculated by single point calculations at the PBE0[98]/Def2-SVP level, which delivers better agreement to the experimentally available phosphorescence data.

Assuming that **M** designates any metal, **Y** any halogen ligand and **X** the whole neutral ligand (phosphine or NHC) shell, E_{Prep} and E_{Bond} energies discussed below are defined as follows: $E_{Prep.}$ is the energy cost afforded by the bare 8-electron $[\mathbf{M_{13}}]^{x+}$ metal core to go from its equilibrium structure to that it adopts in the equilibrium structure of the ligated $\mathbf{M_{13}}$-**X** or $\mathbf{M_{13}Y_n}$-**X** clusters. E_{Bond} is calculated according to the following equations in which all of the considered (frozen) fragment structures are taken from the $\mathbf{M_{13}}$-**X** and $\mathbf{M_{13}Y_n}$-**X** optimized geometries. $E_{Bond} = E(\boldsymbol{M_{13}}\text{-}\boldsymbol{X}) - E([\boldsymbol{M_{13}}]^{x+}) - E(\boldsymbol{X})$ or $E_{Bond} = E(\boldsymbol{M_{13}Y_n}\text{-}\boldsymbol{X}) - E([\boldsymbol{M_{13}Y_n}]^{(x-n)+}) - E(\boldsymbol{X})$.

3. Results and Discussion

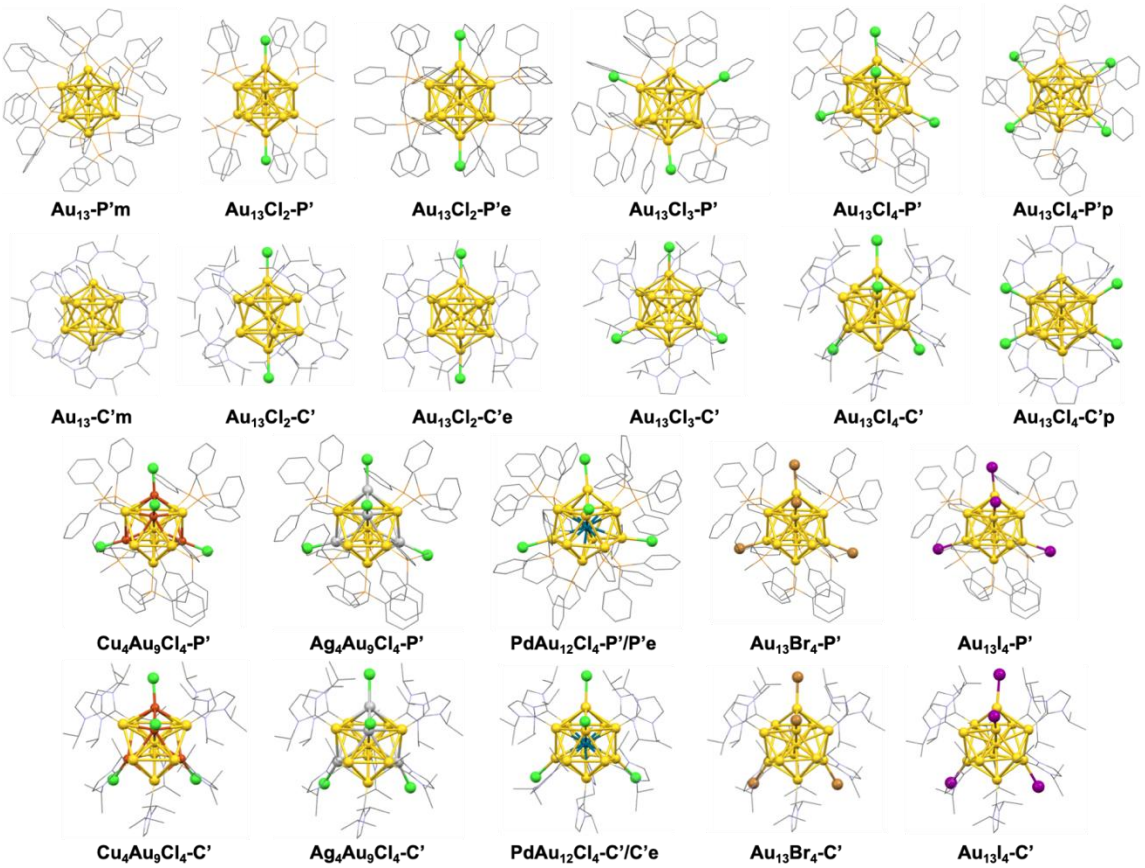

Figure 1. Optimized structures of $\mathbf{M_{13}Y_n}$-**X** (M = Au, Cu, Ag, Pd; Y = Cl, Br, I; *n* = 0, 2-4; X = **P**, **C**). The golden, green, reddish brown, light grey, dark blue, brown and purple spheres are Au, Cl, Cu, Ag, Pd, Br and I atoms, respectively.

The optimized geometries of the phosphine-protected clusters and of their NHC analogues are shown in Figure 1, where for sake of simplicity, M_{13} denotes both monometallic Au_{13} and heterometallic cluster cores. The atomic bond distances of the $\mathbf{M_{13}}$-**P** were found to be in good agreement with their corresponding X-ray structure data (Tables S2-S8). All the

calculated compounds are isoelectronic, with a closed shell *8-ce* $1S^2$ $1P^6$ *superatom* configuration. The HOMO-LUMO gaps of the **M_{13}-P** series are found in the range of 1.4–2.2 eV (Tables S1-S7), which is consistent with the chemical stability of this kind of compound. Interestingly, the **M_{13}-C** compounds show HOMO-LUMO gaps that are slightly larger than that of their **M_{13}-P** counterparts, indicating rather similar stability. The Kohn-Sham frontier molecular orbital diagrams of both **M_{13}-P** and **M_{13}-C** series are shown in Figure 2. The HOMO and LUMO levels are all of 1P and 1D nature, respectively. They are plotted in Figure S1-S11. Unsurprisingly, the frontier orbitals of both the **M_{13}-P** (Figure 2a) and **M_{13}-C** species (Figure 2b) are shifted up in energy when the cluster cationic charge decreases from +5 (**M_{13}-X**) to 0 (**$PdAu_{12}Cl_4$-X'/X'e**). As a consequence, this energy upshift follows the increase of the number of chloride ligands. As a whole, the related electronic structures along with the series, suggest that the hypothetic NHC species should have similar properties as their phosphine relatives, allowing further experimental exploration.

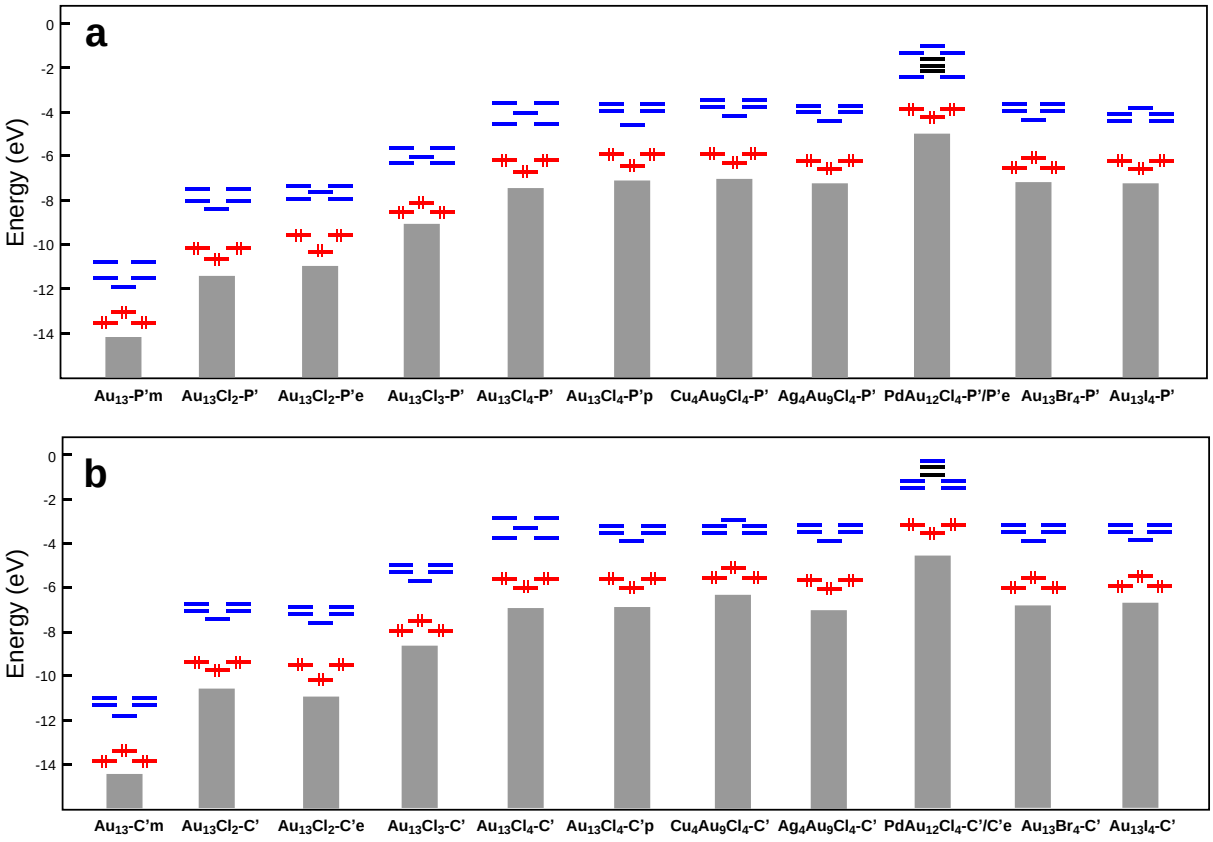

Figure 2. Kohn-Sham frontier molecular orbital diagrams of a) **$M_{13}Y_n$-P** and b) **$M_{13}Y_n$-C** (Y = Cl, Br, I; *n* = 0, 2-4). The grey boxes represent the 5d(Au)-block, the red and blue levels correspond to the *superatomic* 1P and 1D orbitals, respectively.

Thus, the energies of the HOMOs and LUMOs can be tuned by varying the composition of the ligand shell and/or that of the metal core. This capability enables to include such well-defined molecular devices into heterojunction, with more positive or more negative frontier orbital energies with respect to that of the valence band of a semiconductor in a heterojunction array,[99] allowing the control of the location of both electrons and holes in charge transfer mechanisms.

In order to evaluate the stabilizing role of the different ligand shells in the **M_{13}-P** and **M_{13}-C** series, a bonding energy analysis was carried out, not only for the comparison of the energies of interaction between the ligands and metal core, but also for an evaluation of the energy cost associated with the distortion afforded by the metal core upon ligand complexation. To this end, the corresponding bare metal cores were optimized. The energy cost afforded by the bare metal cores to prepare their structure to bond with the ligands (E_{Prep}, see Computational Details) is given in Table 1. The computed E_{Prep} values range between 0.10–0.33 eV, for the gold-halide cores and tend to increase for the doped $M_4Au_9Cl_4$-X' (M = Cu, Ag) species. It is clear that the evaluated E_{Prep} in the **M_{13}-C** series is smaller than those of **M_{13}-P**, which means that the metal cores in **M_{13}-C** species cost less energy to reach their equilibrium states, suggesting that NHC-derivatives exhibit a less rigid ligand-shell, introducing more flexibility to the resulting cluster. This can be useful for studies on cluster core fluxionality, as explored for $Au_{25}(SR)_{18}$ and $Au_{38}(SR)_{24}$ species group.[100,101]

The ligand-core interaction energies for the series evaluated by the computed bonding energies (E_{Bond}, see Computational Details) for the neutral phosphine and NHC ligand shell (Table 1) show that NHCs are slightly more strongly bonded than the phosphine analogues in all the investigated cases, suggesting that NHC-protected gold and gold-rich M_{13} clusters should exhibit a somewhat enhanced thermodynamic stability, which can be useful as ligand-engineering strategy to achieve more stable building-blocks. Interestingly, the **M_{13}-C** cluster cores bear more positive charges than their **M_{13}-P** counterparts (Table 1), as the result of the enhanced core-ligand back-bonding.[102] This is in line with the fact that the frontier orbital energies of the former species are slightly higher than that of the latter (Figure 2). On the other hand, no clear relationship between the core charges and the number of chloride ligands could be traced.

Table 1. Energetic data associated with cluster bonding denoting the cluster core preparation energy (E_{Prep}) and ligand-core interaction (E_{Bond}) (values in eV), and the natural bond order (NBO) charges of the M_{13} core (*q core*, in a.u).

Compound	Corresponding optimized bare metal core	**X = P** E_{Prep}	**X = C** E_{Prep}	**X = P** E_{Bond}	**X = C** E_{Bond}	**X = P** *q core*	**X = C** *q core*
Au_{13}-X'm	$[Au_{13}]^{5+}$ (I_h)	0.19	0.16	-57.79	-62.78	1.35	2.35
$Au_{13}Cl_2$-X'		0.20	0.10	-39.48	-45.44	1.22	2.34
$Au_{13}Cl_2$-X'e		0.32	0.19	-40.50	-44.87	1.47	2.21
$Au_{13}Cl_3$-X'		0.24	0.14	-33.26	-38.61	1.49	2.25
$Au_{13}Cl_4$-X'		0.32	0.21	-27.75	-32.02	1.33	2.21
$Au_{13}Cl_4$-X'p		0.33	0.18	-27.82	-30.87	1.58	2.19
$Au_{13}Br_4$-X'		0.33	0.19	-27.54	-31.58	1.34	2.10
$Au_{13}I_4$-X'		0.31	0.16	-27.13	-30.93	1.11	1.99
$Cu_4Au_9Cl_4$-X'	$[Cu_4Au_9]^{5+}$ (C_{2v})	0.41	0.21	-27.45	-30.80	1.96	2.77
$Ag_4Au_9Cl_4$-X'	$[Ag_4Au_9]^{5+}$ (C_{2v})	0.51	0.40	-27.76	-31.65	1.75	2.59
$PdAu_{12}Cl_4$-X'/X'e	$[PdAu_{12}]^{4+}$ (I_h)	0.28	0.09	-23.36	-27.44	1.45	1.90

The optical properties of AuNCs have been widely explored, owing to their potential use as optical devices,[4,103] which can be tuned by involving different ligands.[48,104–107] In this sense, the variation of the optical properties of the investigated compounds was evaluated with respect to the nature of the cluster core and the different ligand shell. The TD-DFT simulated UV-vis spectra of **M_{13}-P** and **M_{13}-C** series are gathered in Figure 3, and the major computed electronic transition energies associated with them are given in Table 2, together with the corresponding experimental λ_{max} values taken from the literature, where available.

The shapes of the computed UV-vis spectra for the **M_{13}-P** series were found to have a good match with that of the available experimental spectra. In all the cases, the lowest energy band is associated with a transition of mostly (but not exclusively) HOMO → LUMO nature, and in any case is of 1P → 1D metal-to-metal charge transfer (MMCT) nature (see Figures S1-S11). Figure S12 illustrates the energy shift of the lowest energy transition wavelength when going from the phosphine species to their NHC homologues.

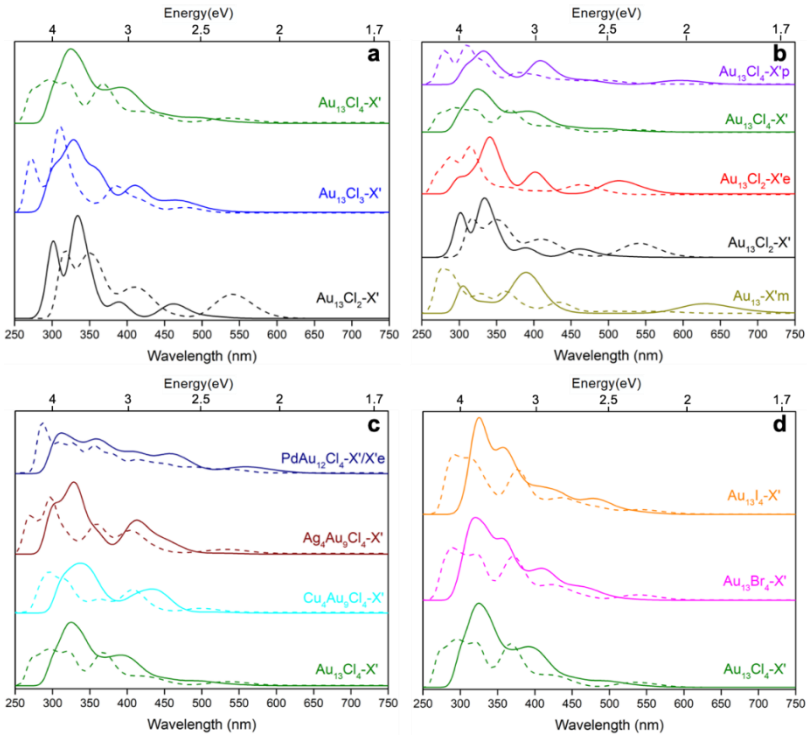

Figure 3. Simulated UV-vis absorption spectra for the computed phosphine derivatives (solid line) and NHC derivatives (dotted line) clusters.

Table 2. Major TD-DFT-Computed UV-Vis excitation energies. Experimental values are also reported, when available in the literature. The Experimental values correspond to the phosphine protected clusters, except for **$Au_{13}Cl_3$-C'**.

Compound	Absorption (nm)			Major character of the low-energy band (X = P, C)
	Exp.	X = P	X = C	
Au_{13}-X'm	700, 440, 300-350(multiple)[a]	625, 387, 304	561(sh$^{\perp}$), 434, 363, 328, 278	1P→1D
$Au_{13}Cl_2$-X'	428, 338, 296[b]	460, 387, 335, 303	540, 409, 352, 319	1P→1D
$Au_{13}Cl_2$-X'e	493, 359, 304 (sh$^{\perp}$)[c]	507, 402, 342, 299 (sh$^{\perp}$)	462, 366, 314, 288	1P→1D
$Au_{13}Cl_3$-X'	490, 420, 330 (X = C)[d]	469, 411, 328	480, 386, 310, 271	1P→1D
$Au_{13}Cl_4$-X'	440, 350, 290 (sh$^{\perp}$)[e]	480, 393, 324	534, 422, 367, 295	1P→1D
$Au_{13}Cl_4$-X'p	430, 340[f]	591, 406, 332	495, 380, 311, 280	1P→1D
$Cu_4Au_9Cl_4$-X'	450, 355, 325 (sh$^{\perp}$)[e]	431, 334	497, 408, 362, 294	1P→1D
$Ag_4Au_9Cl_4$-X'	420, 330, 285 (sh$^{\perp}$)[e]	414, 327, 304 (sh$^{\perp}$)	531, 403, 357, 296, 271(sh$^{\perp}$)	1P→1D
$PdAu_{12}Cl_4$-X'/X'e	–	558, 460, 404 (sh$^{\perp}$), 357, 314	540, 411, 354, 327(sh$^{\perp}$), 308(sh$^{\perp}$) 287	1P→1D
$Au_{13}Br_4$-X'	425, 340, 296 (sh$^{\perp}$)[g]	483, 409, 355, 318	540, 423, 371, 289	1P→1D
$Au_{13}I_4$-X'	–	492, 413, 354, 325	546, 436, 374, 292	1P→1D

Experimental data taken from reference: a) [86]; b) [42]; c) [56]; d) [59]; e) [82]; f) [84]; g) [57]. $^{\perp}$sh = shoulder.

For the homometallic chlorinated **$Au_{13}Cl_n$-P** series, the lowest energy band is red-shifted when increasing the number of Cl atoms from 2 to 4 in both the mono-phosphine (**$Au_{13}Cl_2$-P'**, **$Au_{13}Cl_3$-P'**, **$Au_{13}Cl_4$-P'**) (Figure 3a) and di-phosphine (**$Au_{13}Cl_2$-P'e**, **$Au_{13}Cl_4$-P'p**) (Figure 3b) **$Au_{13}Cl_n$-P** series. The same trend is also found for the **$Au_{13}Cl_n$-C** species (**$Au_{13}Cl_3$-C'**, **$Au_{13}Cl_4$-C'**, **$Au_{13}Cl_2$-C'e**, **$Au_{13}Cl_4$-C'p**), except in the case of **$Au_{13}Cl_2$-C'**. When switching the ligands from mono-phosphines to di-phosphines, the lowest energy band is red-shifted in the **$Au_{13}Cl_n$-P** (n = 2, 4) series, but blue-shifted in the **$Au_{13}Cl_n$-C** (n = 2, 4) series (Figure 3b). When going from the mono-phosphine-protected **$Au_{13}Cl_n$-P** (**$Au_{13}Cl_3$-P'**, **$Au_{13}Cl_4$-P'**) to the mono-NHC-protected **$Au_{13}Cl_n$-C** (**$Au_{13}Cl_3$-C'**, **$Au_{13}Cl_4$-C'**), the lowest energy band is slightly red-shifted, whereas the highest energy band shows a blue-shift tendency (Figure 3a), except in the case of **$Au_{13}Cl_2$-X'** (X = **P**, **C**), in which the whole UV-vis spectra is red-shifted. This trend was also found for the other two halide **$Au_{13}Y_4$-X'** (Y = Br, I; X = **P**, **C**) (Figure 3d) and alloyed **M_4Au_9-X'** (M = Cu, Ag; X = **P**, **C**) series, but not for the case of the palladium-doped species (**$PdAu_{12}$-P'/P'e** and **$PdAu_{12}$-C'/C'e**), where the whole UV-vis spectra are blue-shifted (Figure 3c). From the di-phosphine-protected **$Au_{13}Cl_n$-P** (**$Au_{13}Cl_2$-P'e**, **$Au_{13}Cl_4$-P'p**) to the di-NHC-protected **$Au_{13}Cl_n$-C** (**$Au_{13}Cl_2$-C'e**, **$Au_{13}Cl_4$-C'p**), the whole UV-vis spectrum exhibits a systematic blue-shift tendency, and the same trend is also found for the homoleptic $[Au_{13}(dppm)_6]^{5+}$ (**Au_{13}-P'm**) clusters (Figure 3b). Such features depict the possibility to achieve a fine-tuning of optical absorption properties of the isoelectronic species. Moreover, for the chloride/phosphine protected alloy clusters **$M_4Au_9Cl_4$-P'** (M = Au, Cu, Ag), the magnitude of the lowest energy band blue-shift follows the order **$Ag_4Au_9Cl_4$-P' < $Cu_4Au_9Cl_4$-P' < $Au_{13}Cl_4$-P'**, whereas the order within the NHC analogues, **$Ag_4Au_9Cl_4$-C'** and **$Cu_4Au_9Cl_4$-C'**, is inverted (Figure 3c).

Finally, for the three different halogen protected **$Au_{13}Y_4$-X'** (Y = Cl, Br, I; X = **P**, **C**) species, the lowest energy band shows a small systematic red-shift from Cl to Br to I for both phosphine and NHC analogues, which is consistent with the previous experimental observation on $[Au_{13}(dppe_5)Y_2]^{3+}$ (Y = Cl, Br, I) clusters.[108] Thus, it could be assumed that this red-shift in the lowest energy band is turned to occur in any halogen-protected Au_{13} *superatomic* cluster system, independently from the number of halogenide ligands.

In a subsequent step, owing to the relevant photoluminescent properties of $[Au_{13}(dppe)_5Cl_2]^{3+}$,[55,56] ascribed to a phosphorescent emission originating from the $T_1 \rightarrow S_0$ decay,[55] we have also explored the potential phosphorescent emission of all the investigated species. The $T_1 \rightarrow S_0$ emission[55] exhibits a mixed 1P→1D and 5d(Au)→1D character, thus mainly centered on the metal core. The reported emission for $[Au_{13}(dppe)_5Cl_2]^{3+}$ is observed

at 1.26 eV (982 nm),[55] which is calculated at 1.47 eV (Table 3). Along with the phosphine-protected series, the calculated values range from 0.67 eV (1850 nm) to 1.61 eV (770 nm), in the $Au_{13}Y_n$ species, and from 1.31 eV (946 nm) to 1.53 eV (810 nm) in the doped clusters. In the case of their NHC counterparts, the emission is, in general, blue-shifted, with marked exceptions given by alloyed species and the Br- and I-ligated clusters ($Au_{13}Br_4$ and $Au_{13}I_4$ cores).

In the **$Au_{13}Y_4$-P'** series (Y = Cl, Br, I), a blue-shift is suggested from 1.12 eV (1107 nm) to 1.61 eV (770 nm) when phosphine ligands are involved, and a red-shift for carbene species, from 1.22 eV (1016 nm) to 1.09 eV (1137 nm) (Table 3). Thus, the effect of ligand replacement may be evaluated for each species, suggesting that despite being isolobal ligands,[109] fine modifications and variations can be found between phosphine- and carbene-protected clusters. For the homometallic clusters, a blue-shift of the emission is observed when phosphine-based ligands are replaced by carbenes. However, a red-shift is generally found for the doped species ($M_4Au_9Cl_4$ cores, M = Cu and Ag). Figure S13 illustrates the shift of the phosphorescence emission wavelength when going from the phosphine species to their NHC homologues.

The fluorescence emission of these phosphine- and NHC- species were also investigated (Table 4). For both series, the computed fluorescence emission energies are in the near-infrared region. The NHC series shows comparable emission wavelengths with their phosphine derivatives, except the **Au_{13}-P'm**, **$Au_{13}Cl_2$-P'** and **$Au_{13}Cl_4$-P'p**. For the di-phosphine protected **Au_{13}-P'm** and **$Au_{13}Cl_2$-P'** clusters, an obvious blue-shift of the emission wavelength is observed when replacing phosphines by NHCs. However, a big red-shift of the emission wavelength was found when going from **$Au_{13}Cl_2$-P'** to **$Au_{13}Cl_2$-C'**. In the **$Au_{13}Y_4$-P'** series (Y = Cl, Br, I), a blue-shift of the fluorescence emission was found when going from Cl to Br to I, but their corresponding NHC species show an opposite trend. Figure S14 illustrates the shift of the fluorescence emission wavelength when going from the phosphine species to their NHC homologues.

Table 3. DFT-computed hypothetical phosphorescence emissions.

Compound	$E_{emission}$	Compound	$E_{emission}$
Au_{13}-P'm	0.92 eV (1347 nm)	**Au_{13}-C'm**	1.72 eV (721 nm)
$Au_{13}Cl_2$-P'	1.33 eV (932 nm)	**$Au_{13}Cl_2$-C'**	1.54 eV (805 nm)
$Au_{13}Cl_2$-P'e	1.47 eV (843 nm)	**$Au_{13}Cl_2$-C'e**	1.43 eV (867 nm)
$Au_{13}Cl_3$-P'	1.39 eV (892 nm)	**$Au_{13}Cl_3$-C'**	1.79 eV (693 nm)
$Au_{13}Cl_4$-P'	1.12 eV (1107 nm)	**$Au_{13}Cl_4$-C'**	1.22 eV (1016 nm)
$Au_{13}Cl_4$-P'p	0.67 eV (1850 nm)	**$Au_{13}Cl_4$-C'p**	1.26 eV (984 nm)
$Cu_4Au_9Cl_4$-P'	1.53 eV (810 nm)	**$Cu_4Au_9Cl_4$-C'**	1.14 eV (1087 nm)
$Ag_4Au_9Cl_4$-P'	1.37 eV (905 nm)	**$Ag_4Au_9Cl_4$-C'**	1.34 eV (925 nm)
$PdAu_{12}$Cl4-P	1.31 eV (946 nm)	**$PdAu_{12}$Cl4-C**	1.13 eV (1097 nm)
$Au_{13}Br_4$-P'	1.56 eV (795 nm)	**$Au_{13}Br_4$-C'**	1.17 eV (1059 nm)
$Au_{13}I_4$-P'	1.61 eV (770 nm)	**$Au_{13}I_4$-C'**	1.09 eV (1137 nm)

Table 4. DFT-computed hypothetical fluorescence emissions.

Compound	$E_{emission}$	Compound	$E_{emission}$
Au_{13}-P'm	0.89 eV (1387 nm)	**Au_{13}-C'm**	1.25 eV (988 nm)
$Au_{13}Cl_2$-P'	1.52eV (814 nm)	**$Au_{13}Cl_2$-C'**	0.98 eV (1258 nm)
$Au_{13}Cl_2$-P'e	1.44eV (863 nm)	**$Au_{13}Cl_2$-C'e**	1.60eV (773 nm)
$Au_{13}Cl_3$-P'	1.72 eV (720 nm)	**$Au_{13}Cl_3$-C'**	1.59eV (779 nm)
$Au_{13}Cl_4$-P'	1.15 eV (1075 nm)	**$Au_{13}Cl_4$-C'**	1.16 eV (1069 nm)
$Au_{13}Cl_4$-P'p	0.86 eV (1444 nm)	**$Au_{13}Cl_4$-C'p**	1.27 eV (974 nm)
$Cu_4Au_9Cl_4$-P'	1.53 eV (807 nm)	**$Cu_4Au_9Cl_4$-C'**	1.36 eV (911 nm)
$Ag_4Au_9Cl_4$-P'	1.24 eV (996 nm)	**$Ag_4Au_9Cl_4$-C'**	1.30 eV (954 nm)
$PdAu_{12}$Cl4-P	1.25 eV (989 nm)	**$PdAu_{12}$Cl4-C**	1.55 eV (798 nm)
$Au_{13}Br_4$-P'	1.29 eV (959 nm)	**$Au_{13}Br_4$-C'**	1.09 eV (1128 nm)
$Au_{13}I_4$-P'	1.55 eV (802 nm)	**$Au_{13}I_4$-C'**	1.03 eV (1208 nm)

Conclusions

The similar bonding features of phosphines and N-heterocyclic carbene (NHC) ligands in atomically precise gold nanoclusters (AuNCs) allow to further estimate their role in the modification of the molecular properties of different cluster cores. Based on a wide range of experimentally characterized *8-ce* superatoms, with Au_{13} and M_4Au_9 cores (M = Cu, Ag) decorated with phosphine or halogen and phosphine ligands, the substitution of phosphines by NHCs only marginally perturb the electronic structure, leading to roughly similar optical and luminescent properties, but with interesting modifications. For example, with monodentate ligands, the lowest energy absorption wavelength is red-shifted when going from phosphines to NHCs (see Figure S12). This is the consequence of a lesser HOMO → LUMO contribution to this 1P → 1D transition in the NHC series. With bidentate ligands, the opposite effect, *i.e.*, a blue shift occurs when going from phosphines to NHCs, which is related to the stronger

chelating (distorting) effect of diphosphines on the metal core. These UV-vis wavelength shifts are retained for the chelated species in the emission wavelengths (Figures S13 and S14), but somewhat blurred in the case of the non-chelated ones.

Our results allow us to propose medium-sized species based on gold or gold-rich M_{13} icosahedral core, supporting the feasible obtention of novel targets for explorative synthetic efforts featuring NHC-ligands. Moreover, the addition of successive halogen ligands to the cluster core, leads to a more electron-deficient core, enabling further modification of the frontier orbital energies useful in the design of devices in heterojunction arrays.

ASSOCIATED CONTENT

Supporting Information

Cartesian coordinates of the investigated compounds (in .xyz format). Tables of complementary computed data. Plots of the frontier orbitals. Graphical representations of the computed UV-vis and photoluminescence transition wavelengths.

AUTHOR INFORMATION

Corresponding Authors

Jean-François Halet

jean-francois.halet@univ-rennes1.fr

Jean-Yves Saillard

jean-yves.saillard@univ-rennes1.fr

Alvaro Muñoz-Castro

alvaro.munoz@uautonoma.cl

Author Contributions

The manuscript was written through contributions of all authors. All authors have given approval to the final version of the manuscript.

ACKNOWLEDGMENTS

The authors are grateful to the Chilean-French ECOS-CONYCYT program (project C18E04) and to the French-Chilean International Associated Laboratory for “Multifunctional Molecules and Materials” (LIA-CNRS N°1027). The GENCI (Grand Equipment National de Calcul Intensif) is acknowledged for HCP support (project a0010807367). J. W. thanks the

China Scholarship Council for a Ph.D. scholarship. A.M.-C. acknowledges support from Fondecyt 1180683.

References

(1) Jin, R.; Zeng, C.; Zhou, M.; Chen, Y. Atomically Precise Colloidal Metal Nanoclusters and Nanoparticles: Fundamentals and Opportunities. *Chem. Rev.* **2016**, *116* (18), 10346–10413. https://doi.org/10.1021/acs.chemrev.5b00703.

(2) Du, Y.; Sheng, H.; Astruc, D.; Zhu, M. Atomically Precise Noble Metal Nanoclusters as Efficient Catalysts: A Bridge between Structure and Properties. *Chem. Rev.* **2020**, *120* (2), 526–622. https://doi.org/10.1021/acs.chemrev.8b00726.

(3) Du, X.; Jin, R. Atomically Precise Metal Nanoclusters for Catalysis. *ACS Nano* **2019**, *13* (7), 7383–7387. https://doi.org/10.1021/acsnano.9b04533.

(4) Jin, R. Atomically Precise Metal Nanoclusters: Stable Sizes and Optical Properties. *Nanoscale* **2015**, *7* (5), 1549–1565. https://doi.org/10.1039/C4NR05794E.

(5) Kang, X.; Li, Y.; Zhu, M.; Jin, R. Atomically Precise Alloy Nanoclusters: Syntheses, Structures, and Properties. *Chem. Soc. Rev.* **2020**, *49* (17), 6443–6514. https://doi.org/10.1039/C9CS00633H.

(6) Mingos, D. M. P. Electron Counting Rules for Gold Clusters Which Are Stereochemically Non-Rigid and Exhibit Skeletal Isomerism. In *Structure and Bonding* (Mingos D. M. P. ed.); Springer Berlin Heidelberg: Berlin, Heidelberg, 2021; pp 1–67. https://doi.org/10.1007/430_2021_87.

(7) Hirai, H.; Ito, S.; Takano, S.; Koyasu, K.; Tsukuda, T. Ligand-Protected Gold/Silver Superatoms: Current Status and Emerging Trends. *Chem. Sci.* **2020**, *11* (45), 12233–12248. https://doi.org/10.1039/D0SC04100A.

(8) Reber, A. C.; Khanna, S. N. Superatoms: Electronic and Geometric Effects on Reactivity. *Acc. Chem. Res.* **2017**, *50* (2), 255–263. https://doi.org/10.1021/acs.accounts.6b00464.

(9) Hirata, K.; Tomihara, R.; Kim, K.; Koyasu, K.; Tsukuda, T. Characterization of Chemically Modified Gold and Silver Clusters in Gas Phase. *Phys. Chem. Chem. Phys.* **2019**, *21* (32), 17463–17474. https://doi.org/10.1039/C9CP02622C.

(10) Hasegawa, S.; Takano, S.; Yamazoe, S.; Tsukuda, T. Prominent Hydrogenation Catalysis of a PVP-Stabilized Au_{34} Superatom Provided by Doping a Single Rh Atom. *Chem. Commun.* **2018**, *54* (46), 5915–5918. https://doi.org/10.1039/C8CC03123A.

(11) Sharma, S.; Yamazoe, S.; Ono, T.; Kurashige, W.; Niihori, Y.; Nobusada, K.; Tsukuda, T.; Negishi, Y. Tuning the Electronic Structure of Thiolate-Protected 25-Atom Clusters

by Co-Substitution with Metals Having Different Preferential Sites. *Dalton Trans.* **2016**, *45* (45), 18064–18068. https://doi.org/10.1039/C6DT03214A.

(12) Negishi, Y.; Kurashige, W.; Niihori, Y.; Nobusada, K. Toward the Creation of Stable, Functionalized Metal Clusters. *Phys. Chem. Chem. Phys.* **2013**, *15* (43), 18736. https://doi.org/10.1039/c3cp52837e.

(13) Yamazoe, S.; Tsukuda, T. Metal Clusters in Catalysis. In *Functional Nanometer-Sized Clusters of Transition Metals: Synthesis, Properties and Applications*; Chen, W., Chen, S., Eds.; 2014; pp 291–322. https://doi.org/10.1039/9781782628514-00291.

(14) Yuan, X.; Yao, Q.; Yu, Y.; Luo, Z.; Xie, J. Novel Synthetic Strategies for Thiolate-Protected Au and Ag Nanoclusters: Towards Atomic Precision and Strong Luminescence. In *Functional Nanometer-Sized Clusters of Transition Metals: Synthesis, Properties and Applications*; Chen, W., Chen, S., Eds.; 2014; pp 131–168. https://doi.org/10.1039/9781782628514-00131.

(15) Kawawaki, T.; Kataoka, Y.; Ozaki, S.; Kawachi, M.; Hirata, M.; Negishi, Y. Creation of Active Water-Splitting Photocatalysts by Controlling Cocatalysts Using Atomically Precise Metal Nanoclusters. *Chem. Commun.* **2021**, *57* (4), 417–440. https://doi.org/10.1039/D0CC06809H.

(16) Rao, C. N. R.; Müller, A.; Cheetham, A. K. *The Chemistry of Nanomaterials*; Rao, C. N. R., Müller, A., Cheetham, A. K., Eds.; Wiley-VCH Verlag GmbH & Co. KGaA: Weinheim, FRG, 2004. https://doi.org/10.1002/352760247X.

(17) Sun, Y. Shape-Controlled Synthesis of Gold and Silver Nanoparticles. *Science* **2002**, *298* (5601), 2176–2179. https://doi.org/10.1126/science.1077229.

(18) Yin, Y.; Talapin, D. The Chemistry of Functional Nanomaterials. *Chem. Soc. Rev.* **2013**, *42* (7), 2484–2487. https://doi.org/10.1039/c3cs90011h.

(19) Kurashige, W.; Niihori, Y.; Sharma, S.; Negishi, Y. Precise Synthesis, Functionalization and Application of Thiolate-Protected Gold Clusters. *Coord. Chem. Rev.* **2016**, *320–321*, 238–250. https://doi.org/10.1016/j.ccr.2016.02.013.

(20) Fernando, A.; Weerawardene, K. L. D. M.; Karimova, N. V.; Aikens, C. M. Quantum Mechanical Studies of Large Metal, Metal Oxide, and Metal Chalcogenide Nanoparticles and Clusters. *Chem. Rev.* **2015**, *115* (12), 6112–6216. https://doi.org/10.1021/cr500506r.

(21) Stoll, T.; Sgrò, E.; Jarrett, J. W.; Réhault, J.; Oriana, A.; Sala, L.; Branchi, F.; Cerullo, G.; Knappenberger, K. L. Superatom State-Resolved Dynamics of the Au25(SC8H9)18- Cluster from Two-Dimensional Electronic Spectroscopy. *J. Am.*

Chem. Soc. **2016**, *138* (6), 1788–1791. https://doi.org/10.1021/jacs.5b12621.

(22) Costi, R.; Saunders, A. E.; Banin, U. Colloidal Hybrid Nanostructures: A New Type of Functional Materials. *Angew. Chem. Int. Ed.* **2010**, *49* (29), 4878–4897. https://doi.org/10.1002/anie.200906010.

(23) Cowan, M. J.; Nagarajan, A. V.; Mpourmpakis, G. Correlating Structural Rules with Electronic Properties of Ligand-Protected Alloy Nanoclusters. *J. Chem. Phys.* **2021**, *155* (2), 024303. https://doi.org/10.1063/5.0056690.

(24) Qian, H.; Zhu, Y.; Jin, R. Size-Focusing Synthesis, Optical and Electrochemical Properties of Monodisperse $Au_{38}(SC_2H_4Ph)$ 24 Nanoclusters. *ACS Nano* **2009**, *3* (11), 3795–3803.

(25) Whetten, R. L.; Khoury, J. T.; Alvarez, M. M.; Murthy, S.; Vezmar, I.; Wang, Z. L.; Stephens, P. W.; Cleveland, C. L.; Luedtke, W. D.; Landman, U. Nanocrystal Gold Molecules. *Adv. Mater.* **1996**, *8* (5), 428–433.

(26) Oro, L. A.; Braunstein, P.; Raithby, P. R. *Metal Clusters in Chemistry*; Wiley-vch Weinheim, Germany, 1999; Vol. 3.

(27) Daniel, M.-C.; Astruc, D. Gold Nanoparticles: Assembly, Supramolecular Chemistry, Quantum-Size-Related Properties, and Applications toward Biology, Catalysis, and Nanotechnology. *Chem. Rev.* **2004**, *104* (1), 293–346. https://doi.org/10.1021/cr030698+.

(28) Heaven, M. W.; Dass, A.; White, P. S.; Holt, K. M.; Murray, R. W. Crystal Structure of the Gold Nanoparticle $[N(C_8H_{17})_4][Au_{25}(SCH_2CH_2Ph)_{18}]$. *J. Am. Chem. Soc.* **2008**, *130* (12), 3754–3755. https://doi.org/10.1021/ja800561b.

(29) Walter, M.; Akola, J.; Lopez-Acevedo, O.; Jadzinsky, P. D.; Calero, G.; Ackerson, C. J.; Whetten, R. L.; Grönbeck, H.; Häkkinen, H. A Unified View of Ligand-Protected Gold Clusters as Superatom Complexes. *Proc. Natl. Acad. Sci.* **2008**, *105* (27), 9157–9162. https://doi.org/10.1073/pnas.0801001105.

(30) Jena, P. Beyond the Periodic Table of Elements: The Role of Superatoms. *J. Phys. Chem. Lett.* **2013**, *4* (9), 1432–1442. https://doi.org/10.1021/jz400156t.

(31) Knoppe, S.; Dolamic, I.; Bürgi, T. Racemization of a Chiral Nanoparticle Evidences the Flexibility of the Gold-Thiolate Interface. *J. Am. Chem. Soc.* **2012**, *134* (31), 13114–13120. https://doi.org/10.1021/ja3053865.

(32) Levi-Kalisman, Y.; Jadzinsky, P. D.; Kalisman, N.; Tsunoyama, H.; Tsukuda, T.; Bushnell, D. A.; Kornberg, R. D. Synthesis and Characterization of Au102 (p-MBA) 44 Nanoparticles. *J. Am. Chem. Soc.* **2011**, *133* (9), 2976–2982.

(33) Galloway, J. M.; Bramble, J. P.; Rawlings, A. E.; Burnell, G.; Evans, S. D.; Staniland, S. S. Biotemplated Magnetic Nanoparticle Arrays. *Small* **2012**, *8* (2), 204–208. https://doi.org/10.1002/smll.201101627.

(34) Zeng, C.; Chen, Y.; Das, A.; Jin, R. Transformation Chemistry of Gold Nanoclusters: From One Stable Size to Another. *J. Phys. Chem. Lett.* **2015**, *6* (15), 2976–2986. https://doi.org/10.1021/acs.jpclett.5b01150.

(35) Gao, Y.; Bulusu, S.; Zeng, X. C. A Global Search of Highly Stable Gold-Covered Bimetallic Clusters M@Au_n (n=8–17): Endohedral Gold Clusters. *ChemPhysChem* **2006**, *7* (11), 2275–2278. https://doi.org/10.1002/cphc.200600472.

(36) Pembere, A. M. S.; Cui, C.; Wu, H.; Luo, Z. Small Gold Clusters Catalyzing Oxidant-Free Dehydrogenation of Glycerol Initiated by Methene Hydrogen Atom Transfer. *Chinese Chem. Lett.* **2019**, *30* (5), 1000–1004. https://doi.org/10.1016/j.cclet.2018.12.019.

(37) Ding, W.; Huang, C.; Guan, L.; Liu, X.; Luo, Z.; Li, W. Water-Soluble Au13 Clusters Protected by Binary Thiolates: Structural Accommodation and the Use for Chemosensing. *Chem. Phys. Lett.* **2017**, *676*, 18–24. https://doi.org/10.1016/j.cplett.2017.03.036.

(38) Castleman, A. W.; Khanna, S. N. Clusters, Superatoms, and Building Blocks of New Materials. *J. Phys. Chem. C* **2009**, *113* (7), 2664–2675. https://doi.org/10.1021/jp806850h.

(39) Jadzinsky, P. D.; Calero, G.; Ackerson, C. J.; Bushnell, D. A.; Kornberg, R. D. Structure of a Thiol Monolayer-Protected Gold Nanoparticle at 1.1 Å Resolution. *Science* **2007**, *318* (5849), 430–433. https://doi.org/10.1126/science.1148624.

(40) Claridge, S. A.; Castleman, A. W.; Khanna, S. N.; Murray, C. B.; Sen, A.; Weiss, P. S. Cluster-Assembled Materials. *ACS Nano* **2009**, *3* (2), 244–255. https://doi.org/10.1021/nn800820e.

(41) Bürgi, T. Properties of the Gold-Sulphur Interface: From Self-Assembled Monolayers to Clusters. *Nanoscale* **2015**, *7* (38), 15553–15567. https://doi.org/10.1039/C5NR03497C.

(42) Briant, C. E.; Theobald, B. R. C.; White, J. W.; Bell, L. K.; Mingos, D. M. P.; Welch, A. J. Synthesis and X-Ray Structural Characterization of the Centred Icosahedral Gold Cluster Compound $[Au_{13}(PMe_2Ph)_{10}Cl_2](PF_6)_3$; the Realization of a Theoretical Prediction. *J. Chem. Soc. Chem. Commun.* **1981**, (5), 201–202. https://doi.org/10.1039/c39810000201.

(43) Sheong, F. K.; Zhang, J.-X.; Lin, Z. An $[Au_{13}]^{5+}$ Approach to the Study of Gold Nanoclusters. *Inorg. Chem.* **2016**, *55* (21), 11348–11353. https://doi.org/10.1021/acs.inorgchem.6b01881.

(44) Laupp, M.; Strähle, J. $[(Ph_3PAu)_6(DppeAu_2)(AuCl)_4Pd]$, an Icosahedral Au_{12} Cluster with a Central Pd Atom. *Angew. Chem. Int. Ed.* **1994**, *33* (2), 207–209. https://doi.org/10.1002/anie.199402071.

(45) Kang, X.; Chong, H.; Zhu, M. $Au_{25}(SR)_{18}$: The Captain of the Great Nanocluster Ship. *Nanoscale* **2018**, *10* (23), 10758–10834. https://doi.org/10.1039/C8NR02973C.

(46) Jin, S.; Zhou, M.; Kang, X.; Li, X.; Du, W.; Wei, X.; Chen, S.; Wang, S.; Zhu, M. Three- dimensional Octameric Assembly of Icosahedral M_{13} Units in $[Au_8Ag_{57}(Dppp)_4(C_6H_{11}S)_{32}Cl_2]Cl$ and Its $[Au_8Ag_{55}(Dppp)_4(C_6H_{11}S)_{34}][BPh_4]_2$ Derivative. *Angew. Chem. Int. Ed.* **2020**, *59* (10), 3891–3895. https://doi.org/10.1002/anie.201914350.

(47) Gam, F.; Paez-Hernandez, D.; Arratia-Perez, R.; Liu, C. W. W.; Kahlal, S.; Saillard, J.-Y.; Muñoz-Castro, A. Coinage Metal Superatomic Cores: Insights into Their Intrinsic Stability and Optical Properties from Relativistic DFT Calculations. *Chem. Eur. J.* **2017**, *23* (47), 11330–11337. https://doi.org/10.1002/chem.201701673.

(48) Tsukuda, T.; Häkkinen, H. *Protected Metal Clusters: From Fundamentals to Applications*; Elsevier, 2015.

(49) Saillard, J.-Y.; Halet, J.-F. Structure and Bonding Patterns in Large Molecular Ligated Metal Clusters. *Struct. Bond.* **2016**, *169*, 157–179. https://doi.org/10.1007/430_2015_210.

(50) Fehlner, T.; Halet, J.-F.; Saillard, J.-Y. Molecular Clusters. A Bridge to Solid State Chemistry. *Cambridge Univ. Press. Cambridge, UK.* **2007**.

(51) Häkkinen, H. Atomic and Electronic Structure of Gold Clusters: Understanding Flakes, Cages and Superatoms from Simple Concepts. *Chem. Soc. Rev.* **2008**, *37* (9), 1847–1859. https://doi.org/10.1039/b717686b.

(52) Mäkinen, V.; Koskinen, P.; Häkkinen, H. Modeling Thiolate-Protected Gold Clusters with Density-Functional Tight-Binding. *Eur. Phys. J. D* **2013**, *67* (2), 38. https://doi.org/10.1140/epjd/e2012-30486-4.

(53) Häkkinen, H. Electronic Structure: Shell Structure and the Superatom Concept. In *Protected Metal Clusters: From Fundamentals to Applications*; Hakkinen, H., Tsukuda, T., Eds.; Elsevier Science, 2015; pp 189–222. https://doi.org/10.1016/B978-0-08-100086-1.00008-7.

(54) Lopez-Acevedo, O.; Akola, J.; Whetten, R. L.; Grönbeck, H.; Häkkinen, H. Structure and Bonding in the Ubiquitous Icosahedral Metallic Gold Cluster $Au_{144}(SR)_{60}$. *J. Phys. Chem. C* **2009**, *113* (13), 5035–5038. https://doi.org/10.1021/jp8115098.

(55) Zhang, J.; Zhou, Y.; Zheng, K.; Abroshan, H.; Kauffman, D. R.; Sun, J.; Li, G. Diphosphine-Induced Chiral Propeller Arrangement of Gold Nanoclusters for Singlet Oxygen Photogeneration. *Nano Res.* **2017**, 1–12. https://doi.org/10.1007/s12274-017-1935-2.

(56) Shichibu, Y.; Konishi, K. HCl-Induced Nuclearity Convergence in Diphosphine-Protected Ultrasmall Gold Clusters: A Novel Synthetic Route to "Magic-Number" Au_{13} Clusters. *Small* **2010**, *6* (11), 1216–1220. https://doi.org/10.1002/smll.200902398.

(57) Hall, K. P.; Mingos, D. M. P. Homo- and Heteronuclear Cluster Compounds of Gold. In *Progress in Inorganic Chemistry*; 1984; pp 237–325. https://doi.org/10.1002/9780470166338.ch3.

(58) Ube, H.; Zhang, Q.; Shionoya, M. A Carbon-Centered Hexagold(I) Cluster Supported by N-Heterocyclic Carbene Ligands. *Organometallics* **2018**, *37* (13), 2007–2009. https://doi.org/10.1021/acs.organomet.8b00291.

(59) Narouz, M. R.; Takano, S.; Lummis, P. A.; Levchenko, T. I.; Nazemi, A.; Kaappa, S.; Malola, S.; Yousefalizadeh, G.; Calhoun, L. A.; Stamplecoskie, K. G.; et al. Robust, Highly Luminescent Au_{13} Superatoms Protected by N-Heterocyclic Carbenes. *J. Am. Chem. Soc.* **2019**, *141* (38), 14997–15002. https://doi.org/10.1021/jacs.9b07854.

(60) Munz, D. Pushing Electrons-Which Carbene Ligand for Which Application? *Organometallics* **2018**, *37* (3), 275–289. https://doi.org/10.1021/acs.organomet.7b00720.

(61) Liske, A.; Verlinden, K.; Buhl, H.; Schaper, K.; Ganter, C. Determining the π-Acceptor Properties of N-Heterocyclic Carbenes by Measuring the ^{77}Se NMR Chemical Shifts of Their Selenium Adducts. *Organometallics* **2013**, *32* (19), 5269–5272. https://doi.org/10.1021/om400858y.

(62) Huynh, H. V.; Han, Y.; Jothibasu, R.; Yang, J. A. ^{13}C NMR Spectroscopic Determination of Ligand Donor Strengths Using N-Heterocyclic Carbene Complexes of Palladium(II). *Organometallics* **2009**, *28* (18), 5395–5404. https://doi.org/10.1021/om900667d.

(63) Gusev, D. G.; Peris, E. The Tolman Electronic Parameter (TEP) and the Metal–Metal Electronic Communication in Ditopic NHC Complexes. *Dalton Trans.* **2013**, *42* (20), 7359–7364. https://doi.org/10.1039/c3dt32959c.

(64) Arduengo, A. J.; Bertrand, G. Carbenes Introduction. *Chem. Rev.* **2009**, *109* (8), 3209–3210. https://doi.org/10.1021/cr900241h.

(65) Nelson, D. J.; Nolan, S. P. Quantifying and Understanding the Electronic Properties of N-Heterocyclic Carbenes. *Chem. Soc. Rev.* **2013**, *42* (16), 6723–6753. https://doi.org/10.1039/c3cs60146c.

(66) Muñoz-Castro, A. Potential of N-Heterocyclic Carbene Derivatives from $Au_{13}(Dppe)_5Cl_2$ Gold Superatoms. Evaluation of Electronic, Optical and Chiroptical Properties from Relativistic DFT. *Inorg. Chem. Front.* **2019**, *6* (9), 2349–2358. https://doi.org/10.1039/C9QI00513G.

(67) Li, G.; Abroshan, H.; Liu, C.; Zhuo, S.; Li, Z.; Xie, Y.; Kim, H. J.; Rosi, N. L.; Jin, R. Tailoring the Electronic and Catalytic Properties of Au 25 Nanoclusters via Ligand Engineering. *ACS Nano* **2016**, *10* (8), 7998–8005. https://doi.org/10.1021/acsnano.6b03964.

(68) Yang, H.; Wang, Y.; Lei, J.; Shi, L.; Wu, X.; Mäkinen, V.; Lin, S.; Tang, Z.; He, J.; Häkkinen, H.; et al. Ligand-Stabilized $Au_{13}Cu_x$ (x = 2, 4, 8) Bimetallic Nanoclusters: Ligand Engineering to Control the Exposure of Metal Sites. *J. Am. Chem. Soc.* **2013**, *135* (26), 9568–9571. https://doi.org/10.1021/ja402249s.

(69) Yuan, X.; Goswami, N.; Mathews, I.; Yu, Y.; Xie, J. Enhancing Stability through Ligand-Shell Engineering: A Case Study with $Au_{25}(SR)_{18}$ Nanoclusters. *Nano Res.* **2015**, *8* (11), 3488–3495. https://doi.org/10.1007/s12274-015-0847-2.

(70) Wan, X.-K.; Wang, J.-Q.; Nan, Z.-A.; Wang, Q.-M. Ligand Effects in Catalysis by Atomically Precise Gold Nanoclusters. *Sci. Adv.* **2017**, *3* (10), e1701823. https://doi.org/10.1126/sciadv.1701823.

(71) Karimova, N. V.; Aikens, C. M. Chiroptical Activity in BINAP- and DIOP-Stabilized Octa- and Undecagold Clusters. *J. Phys. Chem. C* **2018**, *122* (20), 11051–11065. https://doi.org/10.1021/acs.jpcc.7b12264.

(72) Yang, Y.; Xu, H.; Cao, D.; Zeng, X. C.; Cheng, D. Hydrogen Production via Efficient Formic Acid Decomposition: Engineering the Surface Structure of Pd-Based Alloy Catalysts by Design. *ACS Catal.* **2019**, *9* (1), 781–790. https://doi.org/10.1021/acscatal.8b03485.

(73) Xu, H.; Cheng, D.; Gao, Y.; Zeng, X. C. Assessment of Catalytic Activities of Gold Nanoclusters with Simple Structure Descriptors. *ACS Catal.* **2018**, *8* (10), 9702–9710. https://doi.org/10.1021/acscatal.8b02423.

(74) Danopoulos, A. A.; Simler, T.; Braunstein, P. N-Heterocyclic Carbene Complexes of

Copper, Nickel, and Cobalt. *Chem. Rev.* **2019**, *119* (6), 3730–3961. https://doi.org/10.1021/acs.chemrev.8b00505.

(75) Ai, P.; Mauro, M.; Gourlaouen, C.; Carrara, S.; De Cola, L.; Tobon, Y.; Giovanella, U.; Botta, C.; Danopoulos, A. A.; Braunstein, P. Bonding, Luminescence, Metallophilicity in Linear Au_3 and Au_2Ag Chains Stabilized by Rigid Diphosphanyl NHC Ligands. *Inorg. Chem.* **2016**, *55* (17), 8527–8542. https://doi.org/10.1021/acs.inorgchem.6b01095.

(76) Ai, P.; Danopoulos, A. A.; Braunstein, P. Aurophilicity-Triggered Assembly of Novel Cyclic Penta- and Hexanuclear Gold(I) Complexes with Rigid Anionic NHC-Type Ligands. *Inorg. Chem.* **2015**, *54* (8), 3722–3724. https://doi.org/10.1021/acs.inorgchem.5b00276.

(77) Hirano, K.; Takano, S.; Tsukuda, T. Ligand Effects on the Structures of $[Au_{23}L_6(C{\equiv}CPh)_9]^{2+}$ (L = N-Heterocyclic Carbene vs Phosphine) with Au_{17} Superatomic Cores. *J. Phys. Chem. C* **2021**, *125* (18), 9930–9936. https://doi.org/10.1021/acs.jpcc.1c02197.

(78) Qi, S.; Ma, Q.; He, X.; Tang, Y. Self-Assembled Monolayers of N-Heterocyclic Carbene on Gold: Stability under Ultrasonic Circumstance and Computational Study. *Colloids Surfaces A Physicochem. Eng. Asp.* **2018**, *538*, 488–493. https://doi.org/10.1016/j.colsurfa.2017.11.041.

(79) Sun, F.; Tang, Q. The Ligand Effect on the Interface Structures and Electrocatalytic Applications of Atomically Precise Metal Nanoclusters. *Nanotechnology* **2021**, *32* (35), 352001. https://doi.org/10.1088/1361-6528/ac027c.

(80) Deng, C.; Chen, J.; Tang, Q. Theoretical Investigation on the Adsorption and Interface Bonding between N-Heterocyclic Carbenes and Metal Surfaces. *J. Phys. Chem. C* **2021**, *125* (8), 4489–4497. https://doi.org/10.1021/acs.jpcc.0c09899.

(81) Wei, J.; Halet, J.-F.; Kahlal, S.; Saillard, J.-Y.; Muñoz-Castro, A. Toward the Formation of N-Heterocyclic-Carbene-Protected Gold Clusters of Various Nuclearities. A Comparison with Their Phosphine-Protected Analogues from Density Functional Theory Calculations. *Inorg. Chem.* **2020**, *59* (20), 15240–15249. https://doi.org/10.1021/acs.inorgchem.0c02219.

(82) Copley, R. C. B.; Mingos, D. M. P. Synthesis and Characterization of the Centred Icosahedral Cluster Series $[Au_9MIB_4Cl_4(PMePh_2)_8][C_2B_9H_{12}]$, Where MIB= Au, Ag or Cu. *J. Chem. Soc. Dalt. Trans.* **1996**, (4), 491–500. https://doi.org/10.1039/dt9960000491.

(83) Shichibu, Y.; Suzuki, K.; Konishi, K. Facile Synthesis and Optical Properties of Magic-Number Au_{13} Clusters. *Nanoscale* **2012**, *4* (14), 4125–4129. https://doi.org/10.1039/c2nr30675a.

(84) Yang, L.; Cheng, H.; Jiang, Y.; Huang, T.; Bao, J.; Sun, Z.; Jiang, Z.; Ma, J.; Sun, F.; Liu, Q.; et al. In Situ Studies on Controlling an Atomically-Accurate Formation Process of Gold Nanoclusters. *Nanoscale* **2015**, *7* (34), 14452–14459. https://doi.org/10.1039/C5NR03711E.

(85) van der Velden, J. W. A.; Vollenbroek, F. A.; Bour, J. J.; Beurskens, P. T.; Smits, J. M. M.; Bosnian, W. P. Gold Clusters Containing Bidentate Phosphine Ligands. Preparation and X-Ray Structure Investigation of $[Au_5(DppmH)_3(Dppm)](NO_3)_2$ and $[Au_{13}(DppmH)_6](NO_3)_n$. *Recl. des Trav. Chim. des Pays-Bas* **1981**, *100* (4), 148–152. https://doi.org/10.1002/recl.19811000404.

(86) Zhang, S.-S.; Feng, L.; Senanayake, R. D.; Aikens, C. M.; Wang, X.-P.; Zhao, Q.-Q.; Tung, C.-H.; Sun, D. Diphosphine-Protected Ultrasmall Gold Nanoclusters: Opened Icosahedral Au_{13} and Heart-Shaped Au_8 Clusters. *Chem. Sci.* **2018**, *9* (5), 1251–1258. https://doi.org/10.1039/C7SC03566G.

(87) Lei, Z.; Pei, X.-L.; Ube, H.; Shionoya, M. Reconstituting C-Centered Hexagold(I) Clusters with N -Heterocyclic Carbene Ligands. *Bull. Chem. Soc. Jpn.* **2021**, *94* (4), 1324–1330. https://doi.org/10.1246/bcsj.20210060.

(88) Frisch, M. J.; Trucks, G. W.; Schlegel, H. B.; Scuseria, G. E.; Robb, M. A.; Cheeseman, J. R.; Scalmani, G.; Barone, V.; Petersson, G. A.; Nakatsuji, H.; et al. Gaussian 16 Revision A.03. 2016.

(89) Becke, A. D. Density-Functional Exchange-Energy Approximation with Correct Asymptotic Behavior. *Phys. Rev. A* **1988**, *38* (6), 3098–3100. https://doi.org/10.1103/PhysRevA.38.3098.

(90) Perdew, J. P. Density-Functional Approximation for the Correlation Energy of the Inhomogeneous Electron Gas. *Phys. Rev. B* **1986**, *33* (12), 8822. https://doi.org/10.1103/PhysRevB.33.8822.

(91) Weigend, F.; Ahlrichs, R. Balanced Basis Sets of Split Valence, Triple Zeta Valence and Quadruple Zeta Valence Quality for H to Rn: Design and Assessment of Accuracy. *Phys. Chem. Chem. Phys.* **2005**, *7* (18), 3297–3305. https://doi.org/10.1039/b508541a.

(92) Grimme, S. Semiempirical GGA-Type Density Functional Constructed with a Long-Range Dispersion Correction. *J. Comput. Chem.* **2006**, *27* (15), 1787–1799. https://doi.org/10.1002/jcc.20495.

(93) Glendening, E. D.; Badenhoop, J. K.; Reed, A. E.; Carpenter, J. E.; Bohmann, J. A.; Morales, C. M.; Landis, C. R.; Weinhold, F. NBO 6.0 Theoretical Chemistry Institute, University of Wisconsin, Madison. **2013**.

(94) Te Velde, G.; Bickelhaupt, F. M.; Baerends, E. J.; Fonseca Guerra, C.; van Gisbergen, S. J. a.; Snijders, J. G.; Ziegler, T.; Velde, G. T. E.; Guerra, C. F.; Gisbergen, S. J. A. Chemistry with ADF. *J. Comput. Chem.* **2001**, *22* (9), 931–967. https://doi.org/10.1002/jcc.1056.

(95) ADF2016, SCM, Theoretical Chemistry, Vrije Universiteit, Amsterdam, The Netherlands. ADF2016, SCM, Theoretical Chemistry, Vrije Universiteit, Amsterdam, The Netherlands.

(96) Stephens, P. J.; Devlin, F. J.; Chabalowski, C. F.; Frisch, M. J. Ab Initio Calculation of Vibrational Absorption and Circular Dichroism Spectra Using Density Functional Force Fields. *J. Phys. Chem.* **1994**, *98* (45), 11623–11627. https://doi.org/10.1021/j100096a001.

(97) Gorelsky, S. I. SWizard Program.

(98) Adamo, C.; Barone, V. Toward Reliable Density Functional Methods without Adjustable Parameters: The PBE0 Model. *J. Chem. Phys.* **1999**, *110* (13), 6158–6170. https://doi.org/10.1063/1.478522.

(99) Marschall, R. Semiconductor Composites: Strategies for Enhancing Charge Carrier Separation to Improve Photocatalytic Activity. *Adv. Funct. Mater.* **2014**, *24* (17), 2421–2440. https://doi.org/10.1002/adfm.201303214.

(100) Pihlajamäki, A.; Hämäläinen, J.; Linja, J.; Nieminen, P.; Malola, S.; Kärkkäinen, T.; Häkkinen, H. Monte Carlo Simulations of $Au_{38}(SCH_3)_{24}$ Nanocluster Using Distance-Based Machine Learning Methods. *J. Phys. Chem. A* **2020**, *124* (23), 4827–4836. https://doi.org/10.1021/acs.jpca.0c01512.

(101) Matus, M. F.; Malola, S.; Kinder Bonilla, E.; Barngrover, B. M.; Aikens, C. M.; Häkkinen, H. A Topological Isomer of the $Au_{25}(SR)_{18}^{-}$ Nanocluster. *Chem. Commun.* **2020**, *56* (58), 8087–8090. https://doi.org/10.1039/D0CC03334K.

(102) MacLeod Carey, D.; Muñoz-Castro, A. Evaluation of N-Heterocyclic Carbene Counterparts of Classical Gold Clusters; Bonding Properties of Octahedral CAu_6, Icosahedral $Au_{13}Cl_2$, and Bi-Icosahedral $Au_{25}Cl_2$ Cores from Relativistic DFT Calcula. *J. Phys. Chem. C* **2019**, *123* (19), 12466–12473. https://doi.org/10.1021/acs.jpcc.9b01254.

(103) Jung, J.; Kang, S.; Han, Y.-K. Ligand Effects on the Stability of Thiol-Stabilized Gold

Nanoclusters: $Au_{25}(SR)_{18}$(-), $Au_{38}(SR)_{24}$, and $Au1_{02}(SR)_{44}$. *Nanoscale* **2012**, *4* (14), 4206–4210. https://doi.org/10.1039/c2nr30501a.

(104) Aikens, C. M. Electronic and Geometric Structure, Optical Properties, and Excited State Behavior in Atomically Precise Thiolate-Stabilized Noble Metal Nanoclusters. *Acc. Chem. Res.* **2018**, *51* (12), 3065–3073. https://doi.org/10.1021/acs.accounts.8b00364.

(105) Weerawardene, K. L. D. M.; Aikens, C. M. Effect of Aliphatic versus Aromatic Ligands on the Structure and Optical Absorption of $Au_{20}(SR)_{16}$. *J. Phys. Chem. C* **2016**, *120* (15), 8354–8363. https://doi.org/10.1021/acs.jpcc.6b01011.

(106) Aikens, C. M. Electronic Structure of Ligand-Passivated Gold and Silver Nanoclusters. *J. Phys. Chem. Lett.* **2011**, *2* (2), 99–104. https://doi.org/10.1021/jz101499g.

(107) Aikens, C. M. Geometric and Electronic Structure of $Au_{25}(SPhX)_{18}^{-}$ (X = H, F, Cl, Br, CH_3, and OCH_3). *J. Phys. Chem. Lett.* **2010**, *1* (17), 2594–2599. https://doi.org/10.1021/jz1009828.

(108) Gao, Z.-H.; Dong, J.; Zhang, Q.-F.; Wang, L.-S. Halogen Effects on the Electronic and Optical Properties of Au_{13} Nanoclusters. *Nanoscale Adv.* **2020**, *2* (10), 4902–4907. https://doi.org/10.1039/D0NA00662A.

(109) Hoffmann, R. Building Bridges Between Inorganic and Organic Chemistry (Nobel Lecture). *Angew. Chem. Int. Ed.* **1982**, *21* (10), 711–724. https://doi.org/10.1002/anie.198207113.

TOC GRAPHICS